Interferometric at-wavelength flare characterization of extreme ultraviolet optical systems

Patrick Naulleau,[a] Kenneth A. Goldberg, and Eric M. Gullikson
Center for X-Ray Optics, Lawrence Berkeley National Laboratory, Berkeley, California 94720

Jeffrey Bokor
Center for X-Ray Optics, Lawrence Berkeley National Laboratory, Berkeley, California 94720 and EECS Department, University of California, Berkeley, California 94720

(Received 2 June 1999; accepted 18 August 1999)

The extreme ultraviolet (EUV) phase-shifting point diffraction interferometer (PS/PDI) has recently been developed to provide the high-accuracy wave-front characterization critical to the development of EUV lithography systems. Here we describe an enhanced implementation of the PS/PDI that significantly extends its measurement bandwidth. The enhanced PS/PDI is capable of simultaneously characterizing both wave front and flare. PS/PDI-based flare characterization of a recently fabricated EUV 10×-reduction lithographic optical system is presented. © *1999 American Vacuum Society.* [S0734-211X(99)09206-9]

I. INTRODUCTION

The quest to develop extreme ultraviolet (EUV) optics for use in next-generation projection lithography systems providing sub-100 nm resolution has led to various innovations in EUV metrology.[1–3] One of these innovations is the EUV phase-shifting point diffraction interferometer (PS/PDI).[3,4] The EUV PS/PDI has been developed to provide the high-accuracy wave-front characterization critical to the development of EUV lithography systems. The reference wave-front accuracy of the PS/PDI has been demonstrated[5,6] to be better than $\lambda_{EUV}/300$ (0.045 nm) within a numerical aperture of 0.082.

For lithographic printing, it is important to consider flare in addition to wave-front error. Flare is the *halo* of light surrounding the optical system point-spread function (PSF), caused by scatter from within the optical system. Previously, the only system-level at-wavelength flare test available for EUV optics involved printing. Recently, an EUV scatterometry-based method has been described.[7] Here we describe a new PS/PDI-based technique that can be performed in parallel with wave-front characterization.

Because PS/PDI-based wave-front metrology measures the wave front at the exit pupil of the optical system, it is equivalent to PSF metrology (the two form a Fourier-transform pair). For this reason, the flare can be characterized using wave-front metrology data if it contains enough spatial-frequency bandwidth, in particular, the mid-spatial-frequency range lying between the ranges commonly referred to as figure and finish. As previously implemented, the PS/PDI was incapable of accurately measuring the extended spatial-frequency band required to characterize flare. Here we describe a modified implementation of the PS/PDI that is designed to meet flare-characterization requirements. The newly developed system is used to characterize a recently fabricated EUV 10×-reduction imaging system.

The interferometric flare-measurement technique described here has advantages over flare-measurement techniques based on roughness characterization of individual optical components[8] because it is an integrated system measurement performed at the operational wavelength. Moreover, the interferometric method requires no additional data collection beyond the data currently collected for EUV wave-front metrology. This aspect is important because the flare measurement imposes no additional test time requirements and it eliminates the need for a separate test device. However, due to measurement-bandwidth limits, the PS/PDI-based system, in practice, has a much lower spatial frequency cutoff than do individual-component roughness characterization techniques. The PS/PDI-based system is thus best suited to measuring short-range flare (covering distances of less than approximately 500 times the diffraction-limited resolution). For a 0.1 μm resolution EUV optical system, this distance is on the order of 50 μm.

II. DESCRIPTION OF THE PHASE-SHIFTING POINT DIFFRACTION INTERFEROMETER

The PS/PDI is briefly described here; more complete descriptions have been previously published.[3,4] The PS/PDI is a variation of the conventional point diffraction interferometer[9,10] in which a transmission grating has been added to greatly improve the optical throughput of the system, and add phase-shifting capability. In the PS/PDI (Fig. 1), the optical system under test is coherently illuminated by a spherical wave generated by diffraction from a pinhole placed in the object plane. To guarantee the quality of the spherical-wave illumination, the pinhole diameter is chosen to be several times smaller than the resolution limit of the optical system. A grating placed either before or after the test optic is used to split the illuminating beam, creating the required test and reference beams. A mask (the PS/PDI mask in Fig. 1) is placed in the image plane of the test optic to block the unwanted diffracted orders generated by the grating and to spatially filter the reference beam using a second pinhole (the reference pinhole), thereby removing the aber-

[a]Electronic mail: pnaulleau@lbl.gov

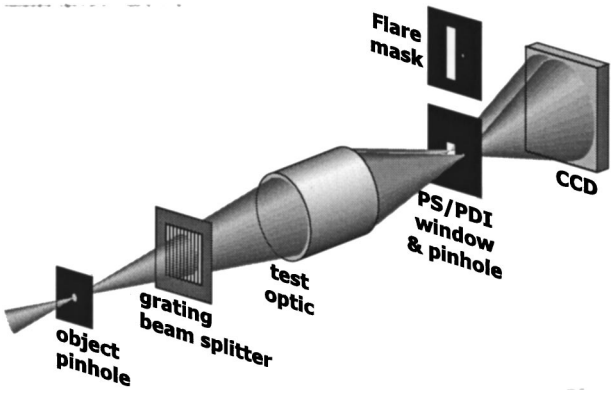

FIG. 1. Schematic of the phase-shifting point diffraction interferometer. Both the wave front and flare-measuring image-plane masks are shown.

rations imparted by the optical system. The test beam, which also contains the aberrations imparted by the optical system, is largely undisturbed by the image-plane mask by virtue of it passing through a window in the PS/PDI mask that is large relative to the diameter of the optical system PSF. The test and reference beams propagate to the mixing plane where they overlap to create an interference pattern recorded on a charge coupled device (CCD) detector.

III. MEASURING FLARE WITH THE PHASE-SHIFTING POINT DIFFRACTION INTERFEROMETER

From the description above, it is apparent that the wave-front measurement bandwidth is limited by the size of the image-plane test-beam window. This bandwidth translates directly to the image-plane distance over which the PS/PDI is capable of measuring flare.

The flare-measurement capabilities of the PS/PDI become more evident when we view the PS/PDI as a system that records an off-axis Fourier-transform hologram[11,12] of the optical system PSF. From this holography point of view the PSF, as seen through the test window, is the *object* distribution. Propagation of the object distribution from the image plane to the CCD in the far field performs the Fourier-transform function. Furthermore, the reference pinhole provides the off-axis reference beam. Reconstruction of this electronic hologram yields an image of the PSF including the tails (halo). The lateral extent of the image is limited to the size of the test window through which it is observed. Thus, the area over which the flare can be determined is simply the area of the test window. In the conventional EUV PS/PDI wave-front measuring configuration, this area is typically a square 3–4.5 μm wide.

To increase the flare measurement range, the image-plane window size must be increased. Unambiguous holographic image reconstruction, however, limits the size of the window in the direction of the beam separation to 2/3 times the pinhole-to-window-center separation or smaller.[11,13] The optimal window configuration for measuring the flare is thus rectangular. In the direction perpendicular to the pinhole separation, where the window can in principle be made arbitrarily long, the flare measurement range is limited by the resolution of the detector and depends on the separation between the image plane and detector. For a detector-to-image-plane separation of 100 mm and a 24 μm detector-element size (typical EUV PS/PDI parameters), this limit corresponds to a full-width measurement range of approximately 50 μm.

Because the PS/PDI derives its reference beam by spatial filtering a laterally displaced copy of the test beam, a significant portion of the scattered light present in the image plane is due to the prefiltered reference beam. Simple holographic image reconstruction would erroneously combine the test and scattered-reference light, yielding a deceptively high measure of the flare. This problem can be overcome using the previously described dual-domain analysis method.[13] The dual-domain method isolates the scattered reference- and test-beam light by recording a set of phase-shifted holograms and processing them in both the temporal and spatial domains.

When the beamsplitter is a binary-amplitude grating, as is typically the case for the EUV PS/PDI, a series of laterally displaced beams is formed in the image plane. These additional beams contribute a small amount of scatter as well. Although the dual-domain method cannot fully eliminate this higher-order corruption, the residual error is relatively small and can be compensated analytically.

IV. EXPERIMENTAL RESULTS

The PS/PDI flare measurement capability has been demonstrated using an EUV 10×-demagnification Schwarzschild objective designed to operate at a wavelength near 13 nm.[14] The interferometry was performed using an undulator beamline[15] at the Advanced Light Source synchrotron radiation facility at Lawrence Berkeley National Laboratory. The beamline provides a tunable source of partially coherent EUV radiation.[16] The tests were performed at a wavelength of 13.4 nm with a bandwidth, $\lambda/\Delta\lambda$, of approximately 350. Here we report the results obtained from a recently fabricated (1998) optic developed to meet a figure specification of better than 0.8 nm and flare specification of less than 5% in a 4 μm line.[17,18]

The flare mask [depicted in Fig. 2(a)] was fabricated using electron-beam lithography and reactive-ion etching. The mask is made of a 200-nm-thick Ni absorbing layer evaporated on a 100-nm-thick Si_3N_4 membrane. The features are etched completely through the membrane prior to the Ni evaporation. This leaves the pinholes and windows completely open in the finished mask, thereby maximizing their transmission. The window sizes are 3×30 μm. Two orthogonal windows are used, allowing anisotropic effects to be measured. Support bars were added to prevent the thin membrane from rupturing. In order to mitigate the obscuring effect of the support bars in the measurement, the reference pinhole is displaced from the window center in the direction parallel to long axis of the window. This in turn allows the test beam to be displaced from the window center during the measurement. A properly chosen displacement eliminates all nulls in the radially averaged PSF data [see also Fig. 2(b)].

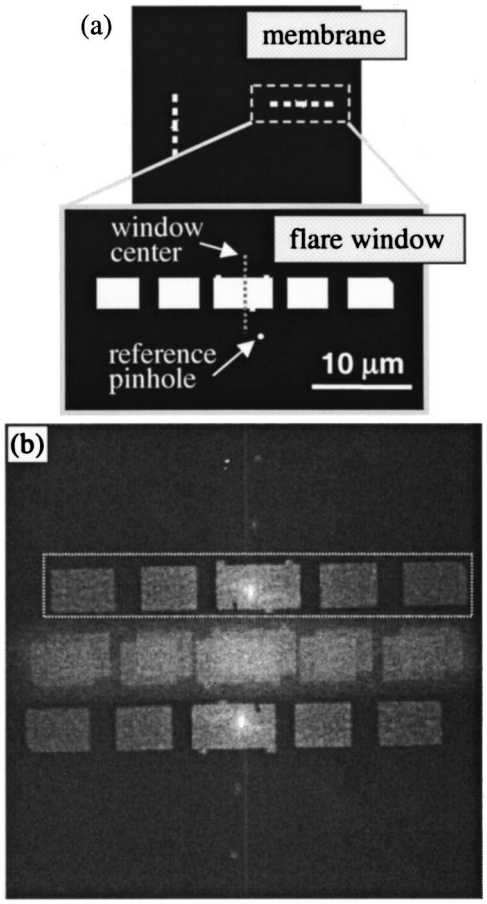

FIG. 2. (a) Schematic of the 3×30 μm flare mask used for the measurement presented here. (b) Logarithmically scaled image of the Fourier transform of a representative hologram from the phase-shifting series. The Fourier-transform image represents the reconstructed image of the image-plane distribution. The dashed line highlights one of the holographic twin images.

Small protrusions are added to the windows (Fig. 2) to act as alignment aids.

The flare-measurement data-collection process involves acquiring a phase-shifting series of holograms (interferograms). The phase shifting is accomplished by lateral translation of the grating beamsplitter between exposures. Figure 2(b) shows a logarithmically scaled image of the Fourier transform of a representative hologram from the phase-shifting series. Because these are Fourier-transform holograms, Fig. 2(b) represents the reconstructed image of the image-plane distribution. The reconstructed image contains the customary twin images and intermodulation image.[11] The dashed line in Fig. 2(b) highlights one of the twin images, in which the image-plane window is clearly visible. The flare is determined by the test-beam portion of the scatter seen in either one of the twin images. Because simple Fourier-transform reconstruction of the PSF cannot distinguish between scatter in the test beam and scatter in the reference beam,[13] the scatter seen in Fig. 2(b) is not an accurate representation of the flare. By design, the reference-beam scatter does not phase shift relative to the pinhole-diffracted reference light; thus, it can be completely eliminated using dual-domain processing.[13] The apparent scatter outside the window region is a result of CCD and photon noise contributions. The mean value of this noise adds a dc bias to the measured scatter energy. This background noise is also present after dual-domain processing and should be removed before determination of the flare. Because the noise is random in nature it cannot be fully eliminated; however, its mean value can readily be removed by measuring and subtracting the average value of the apparent scatter in regions outside the image-plane window.

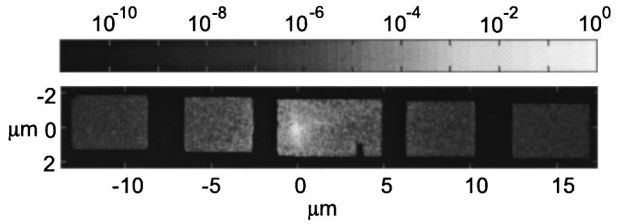

FIG. 3. Logarithmically scaled image of the dual-domain-reconstructed intensity PSF. The PSF shown is an average of three independent measurements. Invalid-data regions are masked.

Figure 3 shows a logarithmically scaled image of the dual-domain-reconstructed intensity PSF. These data were obtained by applying the dual-domain analysis method to the acquired phase-shifting series to recover the complex-amplitude field in the plane of the detector, and then Fourier transforming the field. The PSF shown is an average of three independent measurements. The data dropouts are caused by the bars in the test window. As described above, however, the off-window-center PSF peak ensures that scattering data are available at all radial separations from the PSF peak.

Having calculated the corrected PSF, it is possible to characterize the flare. To this end, we find the normalized scatter-energy density as a function of radial distance from the PSF peak $S(r)$. This is simply the radially averaged PSF

$$S(r)=\frac{1}{2\pi r}\int \mathrm{PSF}(r,\theta)\,d\theta. \tag{1}$$

Performing this calculation on the PSF in Fig. 3 yields an energy density with a radial decay that is well approximated by $r^{-3.10\pm0.01}$.

Because the test window is elongated in one direction only, the scatter-energy-density results may be biased if the scatter is anisotropic. To assess the significance of this potential problem, the measurement is repeated using a window oriented in the orthogonal direction. The orthogonal direction is found to have a scatter-energy radial decay well approximated by $r^{-3.03\pm0.05}$. The small difference between the two directions indicates slight anisotropic scattering effects.

Combining the results from the two orthogonal directions leads to the scatter energy depicted in Fig. 4. The imperfect Airy lobes are caused by aberrations in the optic. In order to predict the flare expected in a typical imaging situation, the scatter-energy density must be known over the full radial extent of the field. For the optics considered here, the full field size is 250 μm radius in the image plane. The extended-range scatter-energy density can be obtained by extrapolation

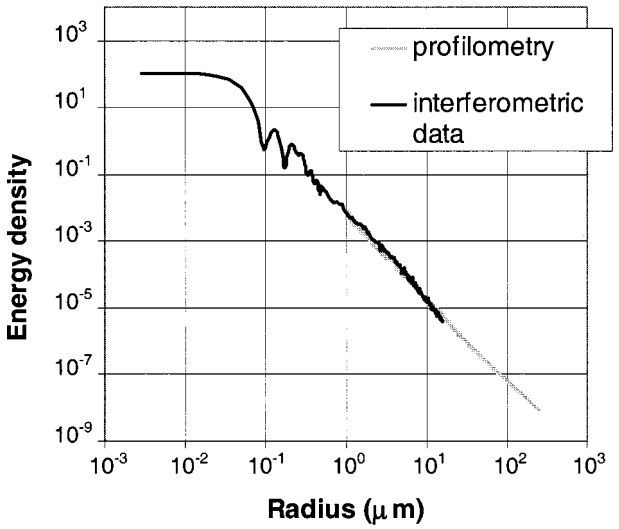

FIG. 4. Comparison of the scatter-energy density as a function of radial separation from the PSF peak determined by the PS/PDI- and profilometry-based methods, respectively.

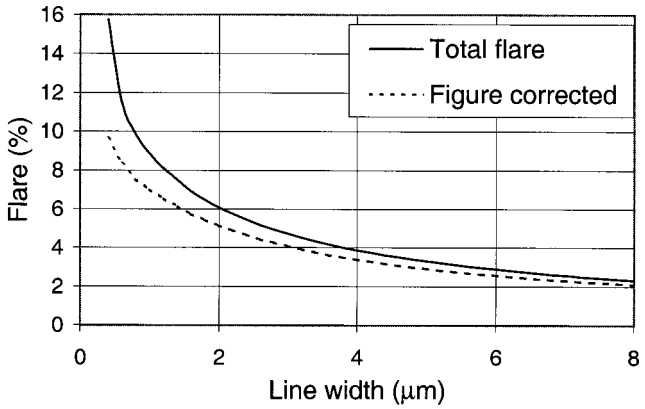

FIG. 5. Calculated flare in an isolated line as a function of linewidth with a 250 μm radius image-field size. Also shown is the *figure-corrected* flare derived by removing the flare that would be calculated given a smooth yet aberrated optic. For the high-quality optics under consideration here, this is essentially the flare one would calculate from an ideal Airy pattern. The figure-corrected flare calls out the flare caused by roughness alone.

of the interferometrically determined data or by use of data derived from profilometry performed on the individual substrates before assembly of the optical system. In order to avoid possible extrapolation errors, we choose the latter. The plot in Fig. 4 shows an overlay of the scatter-energy density predicted from profilometry. The two measurement methods have overlapping data in the radial range from 1 to 16 μm. Good agreement between the two methods is evident.

From the full-field scatter, it is now possible to predict the flare, defined here as

$$\text{flare} = \frac{E_t - E_s}{E_t}, \tag{2}$$

where E_t is the total PSF energy in the field of interest and E_s is the specular energy in the field. We defined the specular energy as the PSF energy contained within the feature size of interest. Figure 5 shows a plot of the flare in an isolated line as a function of linewidth for a 250 μm radius field of view. The flare in a 4 μm line is $3.9\% \pm 0.1\%$, better than the 5% fabrication target for this optic. The flare value predicted by profilometry alone is 4.0%.[7] Also shown in Fig. 5 is the *figure-corrected* flare derived by removing the flare that would be calculated given a smooth yet aberrated optic (figure error only). For the high-quality optics under consideration here, this is essentially the flare one would calculate from the tails of an ideal Airy pattern. Although the figure-corrected flare is not representative of the contrast one might expect in the aerial image, it does call out the flare caused by roughness alone. The roughness-induced flare in a 4 μm line is 3.4%.

The flare measurements presented here were also verified using an EUV scatterometry technique that separately determined the flare to be 4.5%.[7] The scatterometry method works by placing a photodiode behind a field sized aperture in the image plane. A subresolution pinhole in the object plane illuminates the optic coherently. With the diode and aperture centered on the image point, the total energy in the field of interest E_t is measured. The specular component of the beam is found by translating the aperture and diode, and using the aperture edge to perform a *knife-edge test*. This test is conveniently performed in the PS/PDI by replacing the image-plane mask with the aperture-diode combination.

V. CONCLUSION

The measurement bandwidth of the PS/PDI has been significantly extended. This new capability, in turn, allows the PS/PDI to be used as an at-wavelength flare characterization tool. The improved PS/PDI provides a system-level flare test that can be performed in parallel with wave-front metrology. The system has been successfully used to characterize a recently fabricated low-flare 10×-reduction EUV lithographic optic.

ACKNOWLEDGMENTS

The authors are greatly indebted to Erik Anderson for nanofabrication of masks, to Phil Batson for engineering support, and to the entire CXRO staff for enabling this research. Special thanks are due to Paul Denham for expert assistance with experimental control systems. This research was supported by the Extreme Ultraviolet Limited Liability Company, the Semiconductor Research Corporation, DARPA Advanced Lithography Program, and the DOE Office of Basic Energy Science.

[1]J. Bjorkholm *et al.*, J. Vac. Sci. Technol. B **13**, 2919 (1995).
[2]A. Ray-Chaudhuri *et al.*, J. Vac. Sci. Technol. B **13**, 3089 (1995).
[3]H. Medecki *et al.*, Opt. Lett. **21**, 1526 (1996).
[4]K. A. Goldberg, Ph.D. dissertation, University of California, Berkeley, 1997.
[5]P. Naulleau *et al.*, Proc. SPIE **3331**, 114 (1998).
[6]K. Goldberg *et al.*, J. Vac. Sci. Technol. B **16**, 3435 (1998).
[7]E. Gullikson *et al.*, Proc. SPIE **3676**, 717 (1999).

[8]E. M. Gullikson, Proc. SPIE **3331**, 72 (1998).
[9]W. Linnik, Proceedings of the Academy of Science of the USSR, 1933, Vol. 1, p. 210.
[10]R. N. Smartt and W. H. Steel, J. Appl. Phys. **14**, 351 (1975).
[11]E. N. Leith and J. Upatnieks, J. Opt. Soc. Am. **52**, 1123 (1962).
[12]E. N. Leith and J. Upatnieks, J. Opt. Soc. Am. **54**, 1295 (1964).
[13]P. Naulleau and K. A. Goldberg, Appl. Opt. **38**, 3523 (1999).
[14]D. A. Tichenor *et al.*, in *OSA Proceedings on Soft X-Ray Projection Lithography*, edited by A. M. Hawryluk and R. H. Stulen (Optical Society of America, Washington, DC, 1993), Vol. 18, p. 79.
[15]R. Beguiristain *et al.*, Proc. SPIE **2855**, 159 (1996).
[16]D. Attwood *et al.*, IEEE J. Quantum Electron. **35**, 709 (1999).
[17]K. A. Goldberg *et al.*, Proc. SPIE **3676**, 635 (1999).
[18]J. Goldsmith *et al.*, Proc. SPIE **3676**, 264 (1999).